PROCEEDINGS OF SCIENCE

Galactic Cosmic Ray Energy Spectrum for Fe from ~0.8 to ~10 GeV/nuc with the SuperTIGER Instrument

A. W. Labrador[1,*], W. R. Binns[2], R. G. Bose[2], T. J. Brandt[3], P.F. Dowkontt[2], T. Hams[3,6], M. H. Israel[2], J. T. Link[3,6], R. A. Mewaldt[1], J. W. Mitchell[3], R. P. Murphy[2], B. F. Rauch[2], K. Sakai[3,6], M. Sasaki[3,6], E. C. Stone[1], C. J. Waddington[4], J. E. Ward[2], and M. E. Wiedenbeck[5]

1. California Institute of Technology, Pasadena, CA 91125 USA;
2. Washington University, St. Louis, MO 63130 USA;
3. NASA/Goddard Space Flight Center, Greenbelt, MD 20771 USA;
4. The University of Minnesota, Minneapolis, MN 55455, USA:
5. Jet Propulsion Laboratory, California Institute of Technology, Pasadena, CA 91109 USA
6. Center for Research and Exploration in Space Science and Technology (CRESST), Greenbelt, MD 20771, USA

E-mail: labrador@srl.caltech.edu

SuperTIGER (Trans-Iron Galactic Element Recorder) is a large-area balloon-borne instrument built to measure the galactic cosmic-ray abundances of elements from Z=10 (Ne) through Z=56 (Ba) at energies from 0.8 to ~10 GeV/nuc. SuperTIGER successfully flew around Antarctica for a record-breaking 55 days, from December 8, 2012 to February 1, 2013. In this paper, we present results of an analysis of the data taken during the flight for Fe (Z=26). We report on energy calibrations and instrumental and atmospheric corrections to obtain cosmic ray intensities vs. energy, and we will compare selected SuperTIGER galactic cosmic ray Fe spectrum with those from ACE/SIS during the time of the SuperTIGER flight.

35th International Cosmic Ray Conference - ICRC2017
10-20 July, 2017
Bexco, Busan, Korea

PoS(ICRC2017)167

* Speaker

1. Introduction

SuperTIGER (Trans-Iron Galactic Element Recorder) is a large area, balloon-borne experiment designed to measure the galactic cosmic-ray abundances of elements from Ne (Z=10) to Ba (Z=56) at ~0.8–10 GeV/nuc. SuperTIGER had a record-breaking flight of 55 days around Antarctica, from December 8, 2012 to February 1, 2013 [1].

We have previously reported relative abundances of ultraheavy elements ($30 \leq Z \leq 40$) in SuperTIGER data that are consistent with earlier TIGER results and that support galactic cosmic ray origins in OB associations with preferential acceleration of refractory elements over volatile elements [2]. We have also reported relative abundances of iron secondaries, e.g. (Sc+Ti+V)/Fe, that are roughly consistent with HEAO measurements as well as Standard Leaky Box Model calculations [3,4].

In addition to measuring relative abundances of ultraheavy elements and abundant elements, SuperTIGER can measure energy spectra for abundant elements. For example, an investigation that would benefit from the measurement of the Fe energy spectrum in SuperTIGER data would be a search for microquasar signatures. Heinz and Sunyaev [5] suggested that relativistic jets observed in some micro-quasars (e.g. GRS 1915+105 and GRO J1655-40) might produce narrow, near-monoenergetic features in cosmic ray spectra. Figure 1 shows simulated SuperTIGER Fe energy spectra with simulated, near-monoenergetic beams appearing as 1%, 5%, and 10% integrated enhancements above a normal power-law spectrum.

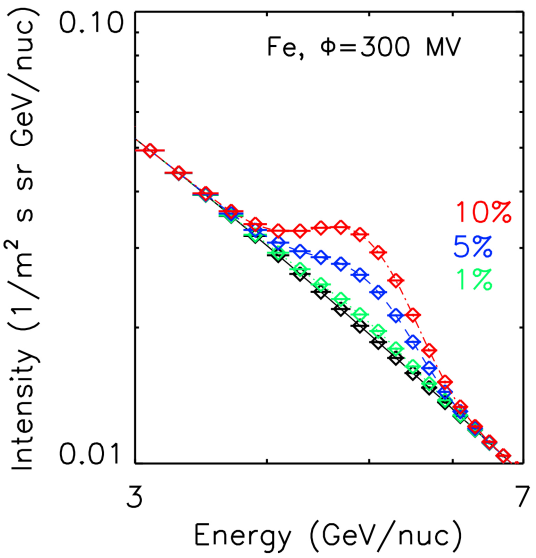

Figure 1: Example of near monoenergetic Fe superimposed atop a normal galactic Fe spectrum. The measurements are simulated for the 2012-2013 SuperTIGER flight. The colored curves represent 1, 5, and 10% integrated enhancements above the normal Fe spectrum integrated from 2.5 to 10 GeV/nc

We report in this paper our current progress in measuring the ~0.8–10 GeV/nuc Fe (Z=26) spectrum for a sample of SuperTIGER flight data. This work will be generally applicable for Z=10–30 element spectra for the entire flight.

2. The SuperTIGER Instrument

SuperTIGER is divided into two nearly identical modules, each of which is a stack of several detectors. From top to bottom, the detectors in each module are a plastic scintillator (S1), a top scintillating optical fiber hodoscope (H1), an aerogel Cherenkov (refractive index n=1.025 or n=1.043) detector (C0), an acrylic Cherenkov (n=1.49) detector (C1), another plastic scintillator (S2), a bottom hodoscope (H2), and a third plastic scintillator (S3). In one module, the aerogel blocks in the C0 detector are entirely n=1.043 refractive index aerogels (threshold energy of ~2.5 GeV/nuc), while in the other module, half of the C0 aerogels have a refractive index n=1.043 while the other half have n=1.025 (threshold energy ~3.3 GeV/nuc). Otherwise, the modules are functionally identical. See Figure 2. The SuperTIGER instrument is described in greater detail by Binns et al. [2].

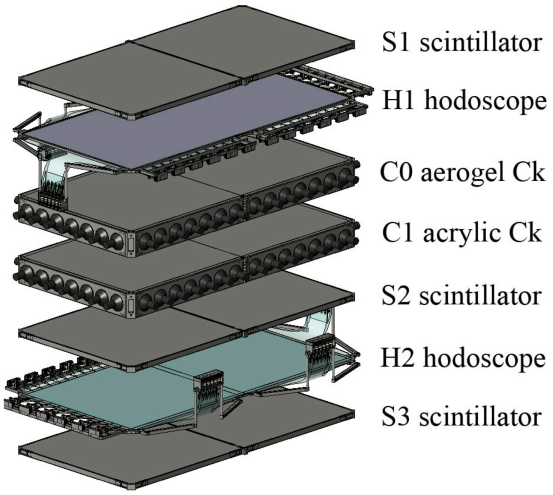

Figure 2: Expanded view of one SuperTIGER module, from Binns et al. [2].

3. Data Analysis

For this preliminary analysis, we examine a sample of the SuperTIGER flight data from 26-28 December 2012. This data set is the line-of-sight (LOS) data telemetered when the experiment could transmit data directly to McMurdo Base. Though a small data set, this data was not processed through the priority system that was employed for the TDRSS data, which means that the LOS data is more complete for Z<30 during its duration.

Particles are identified by charge and velocity through combinations of measurements in the scintillation and Cherenkov detectors (Figures 3a and 3b). The hodoscopes provide particle trajectories for angle- and position-dependent mapping and correction in the data analysis. The axes in Figures 3a and 3b are the scintillator ($S^{1/1.7}$) and Cherenkov ($C0^{1/2}$ and $C1^{1/2}$) signals, scaled to approximately Z for each element at the highest velocities. Element tracks for abundant elements are easily identifiable in each figure, with Fe being the darkest track toward the top of each figure and Mg, Al, and Si tracks being visible near the bottom. From the abundant element tracks, charges for ultraheavey elements may be extrapolated. More rigorous charge determination for the ultra-heavy elements is described in detail by Murphy et al. [2].

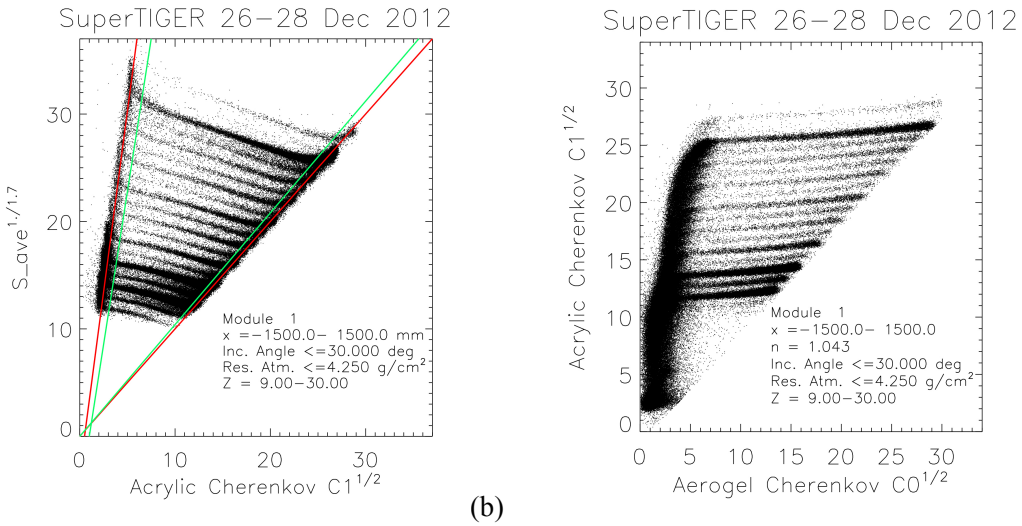

(a) (b)

Figures 3 a (left) and b: Scintillation signal vs. acrylic Cherenkov signal and acrylic Cherenkov signal vs. aerogel Cherenkov signal.

After elements are identified by charge separation from the data shown in Figures 3a and 3b, we obtain velocity ß from the Cherenkov signals with the formula

$$C_{norm} = Z^2 \left[\frac{1-\frac{1}{\beta^2 n^2}}{1-\frac{1}{n^2}} \right] \qquad [1]$$

where Z is the particle charge, n is the Cherenkov radiator index of refraction, and ß is the particle velocity. C_{norm} is the Cherenkov signal, which is expected to vary from 0 to Z^2, depending upon the energy and exceeding zero only when the threshold velocity $ß_{thresh} = 1/n$ is exceeded.

When scaling to the arbitrary scales shown on Figures 3a and 3b, account must be taken of the zero offsets and background at the threshold signal. The background signals contributing to the zero offsets include scintillation signal from mounting or reflecting materials in the Cherenkov counters as well as secondary Cherenkov signals from Goretex reflector and knock-on electrons. In both Figures 3a and 3b, the rightmost boundaries of the data are defined by the

maximum Cherenkov signals in C1 and C0, or maximum velocity $\beta \approx 1$. The left boundaries are defined by background signals below the primary Cherenkov radiator threshold, e.g. dominated by scintillation ($\propto Z^2$) in the C1 counter, and a combination of scintillation (from the thin polyethylene film used to mount the aerogels), knock-on electrons in the aerogels, and Goretex reflector Cherenkov signals in C0.

Figure 3a shows that the establishment of a velocity scale is straightforward, with left and right boundaries of the data defining threshold velocity (ß=1/1.49, or energy 0.33 GeV/nuc at the instrument; zero C0 signal) and the right boundary marking $\beta \approx 1$ in the acrylic Cherenkov signal. These boundaries are marked with red lines in Figure 3a. However, at the upper end of this energy range in Figure 3a, the energies overlap with the aerogel Cherenkov threshold (~2.4 GeV/nuc). Near or below acrylic Cherenkov threshold, particle signals overlap between adjacent charge values (Z). Therefore, events outside of the boundaries marked by the green lines in Figure 3a are either discarded, at low energies, or are analyzed instead with the aerogel Cherenkov signals providing velocity.

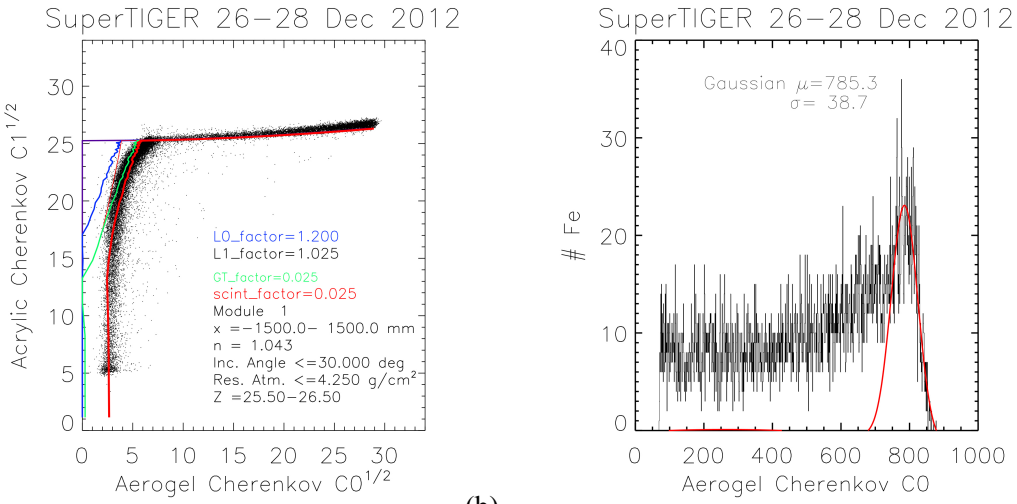

(a) (b)

Figures 4a (left) and 4b: At left are SuperTIGER Fe data points, plotted as acrylic Cherenkov signal vs. aerogel Cherenkov signal. Fits of below-threshold background contributions are shown, including scintillation (bold red) from the plastic film containing the aerogel, Goretex Cherenkov signal (red without knock-on electrons, green with knock-on electrons), and the aerogel Cherenkov signal (with (purple) and without (blue) knock-on electrons). At right is a Gaussian fit to the aerogel Cherenkov signal histogram for Fe at ß=1.

Figures 4a and 4b illustrate how the velocity scales are established in the aerogel Cherenkov energy range. Figure 4a shows SuperTIGER data points for Fe, plotted as acrylic Cherenkov signal vs. aerogel Cherenkov signal. Contributions from scintillation from the plastic film used to wrap and mount the aerogels are shown as the yellow curve, while Cherenkov light

contributions from the Goretex reflector material are shown in red (and green, with knock-on electron signals in the Goretex). The primary aerogel Cherenkov signal is shown in purple, with dark blue showing the knock-on electron contribution from the aerogels. (For all knock-on electron Cherenkov contributions, we used a Monte Carlo simulation derived from calculations by Grove & Mewaldt [6].) Finally, Figure 4b shows a Gaussian fit to the uppermost end of the Fe Cherenkov signal, yielding the $\beta \approx 1$ signal.

4. Preliminary Results

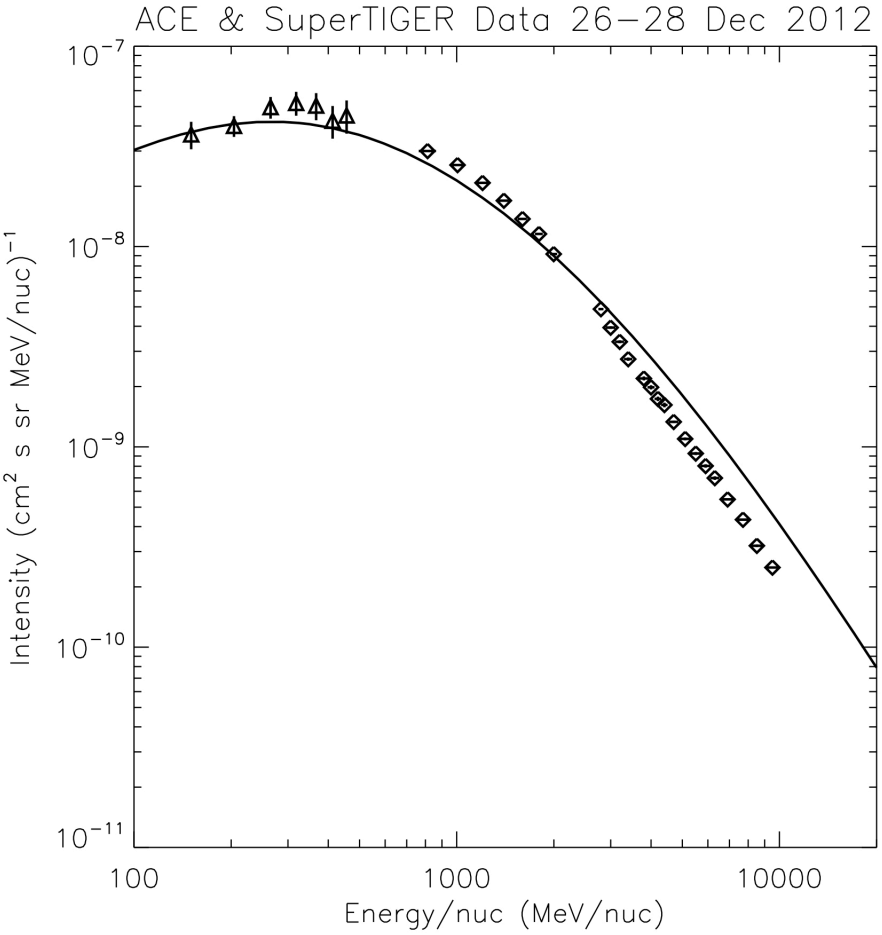

Figure 5: ACE/CRIS Fe intensities (open triangles) during the 26-27 Dec 2012 period [7], with a 1 AU galactic cosmic ray model calculation with a solar modulation parameter $\phi = 575\ MV$. Preliminary SuperTIGER data points for Fe (open diamonds) are scaled to fit the curve. Statistical uncertainties are included but are smaller than the plot symbols; systematic uncertainties await further analysis.

Figure 5 compares ACE/CRIS Fe intensities and a 1 AU galactic cosmic ray Fe model to preliminary SuperTIGER Fe intensities [7,8]. While some calculations and analysis necessary for calculating final SuperTIGER spectra, the SuperTIGER analysis is still ongoing, with some corrections yet to be calculated. As noted in the previous section, velocity and energy calibrations are established for Fe, and related calibrations for other abundant elements should follow in the same way. Energy losses in the instrument and in the residual atmosphere above, during flight, have also been calculated for Fe. However, corrections for interaction losses in the instrument have yet to be fully updated for the materials in SuperTIGER, e.g. the interaction loss corrections for the Fe secondary to primary abundance ratios were calculated using the TIGER configuration as an approximation [3,9]. Also, we have yet to establish corrections for telemetry losses and livetime. Therefore, the SuperTIGER Fe data in Figure 5 are scaled to allow the data points to lie on the model curve.

However, even with the small data sample, the large area of SuperTIGER was enough to collect sufficient Fe during this time period that the SuperTIGER statistical uncertainties are smaller than the plot symbols for most energies. Systematic uncertainties are yet to be determined. Once the instrumental corrections are complete, it appears likely that we will be able to eliminate microquasar signatures at the 5-10% relative intensity level indicated in Figure 1.

Acknowledgements

This work was supported by NASA under grants NNX09AC17G NNX09AC18G, NNX14AB24G, NNX14AB25G, and NNX15AC15G, by the Peggy and Steve Fossett Foundation, and by the McDonnell Center for the Space Sciences at Washington University in St. Louis. We thank the ACE/CRIS instrument team and the ACE Science Center for providing ACE data.

References

[1] W.R. Binns et al, *The SuperTIGER Instrument: Measurements of Elemental Abundances of Ultra-Heavy Galactic Cosmic Rays,* The Astrophysical Journal **788** 18 (June 2014).

[2] R. Murphy et al., *Abundances of Ultra-Heavy Galactic Cosmic Rays from the SuperTIGER Instrument*, Proc. 34th International Cosmic Ray Conference, The Hague (2015).

[3] A.W. Labrador et al., *Galactic Cosmic-Ray Composition and Spectra for Ne through Cu from 0.8 to 10 GeV/nuc with the SuperTIGER Instrument*, Proc. 34th International Cosmic Ray Conference, The Hague (2015).

[4] J.J. Engelmann et al., *Charge composition and energy spectra of cosmic-ray nuclei for elements from Be to Ni. Results from HEAO-3-C2*, Astronomy and Astrophysics **233** 96 (1990).

[5] S. Heinz & R. Sunyaev, *Cosmic rays from microquasars: A narrow component to the CR spectrum?*, Astronomy and Astrophysics, **390** 751 (2002).

[6] J.E. Grove and R.A. Mewaldt. *Nuclear Instruments and Methods in Physics Research*, **A314**, 495 (1992).

[7] ACE Science Center, http://www.srl.caltech.edu/ACE/ASC/level2/index.html.

[8] A.J. Davis, R.A. Mewaldt, W.R. Binns, E.R. Christian, C.M.S. Cohen, A.C. Cummings, J.S. George, P.L. Hink, R.A. Leske, E.C. Stone, T.T. von Rosenvinge, M.E. Wiedenbeck, N.E. Yanasak, *Proceedings of the 27th International Cosmic Ray Conference, Hamburg,* **10**, 3971, 2001.

[9] B. Rauch, *Measurement of the relative abundance of the ultra-heavy galactic cosmic rays (30≤Z≤40) with the Trans-Iron Galactic Element Recorder (TIGER) instrument,* PhD Thesis, Washington University, St. Louis 2008.